

A Machine Learning Approach for Automated Dune Detection and Morphological Metric Calculation on Planetary Surfaces

David Leblanc¹

University of Nevada, Reno, NV 89557

Nicholas Lancaster²

Desert Research Institute, Reno, NV 89512

George Bebis³

University of Nevada, Reno, NV 89557

Mircea Nicolescu⁴

University of Nevada, Reno, NV 89557

Abstract

This is where the abstract will go. TODO

Keywords: Dune Mapping, Machine Learning, Image Processing, Pattern Matching

1. Introduction

2. Study Areas

As part of this research project, two datasets were used in order to prove the robustness of this method. The datasets include a wide range of dune types with varying morphological properties.

¹Graduate Student, University of Nevada, Reno, Department of Computer Science and Engineering

²Research Professor, Desert Research Institute, Division of Earth and Ecosystem Sciences

³Professor and Chair, University of Nevada, Reno, Department of Computer Science and Engineering

⁴Associate Professor, University of Nevada, Reno, Department of Computer Science and Engineering

The data provided in each set are satellite images of dune field regions available through Google Earth and NASA datasets. Included with the images is the ground truth which has been manually labeled by experts in the research field. The ground truth consists of crest-lines for each positive dune detection.

10 In each case, the scales of the satellite images were chosen such that the inter-dune distance appeared roughly normalized across the entire dataset. Scale selection of the images is important process for even comparison of the methods for different regions. The images are resized to an appropriate resolution for processing and even across the entire dataset.

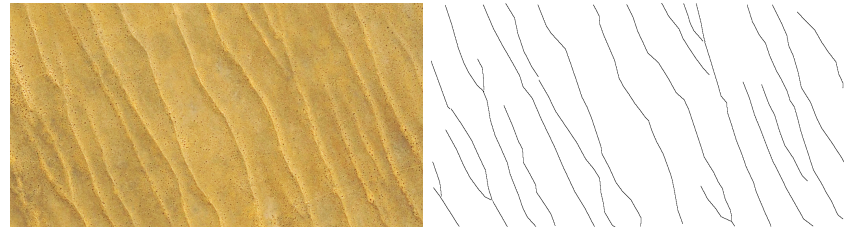
15 The method described in this paper was tested on two distinct datasets: an terrestrial dataset which includes dune fields of various regions on Earth, along with the dataset provided in [1] which is located on Mars in the Ganges crater region. The same method was applied on both datasets.

2.1. Terrestrial Dataset

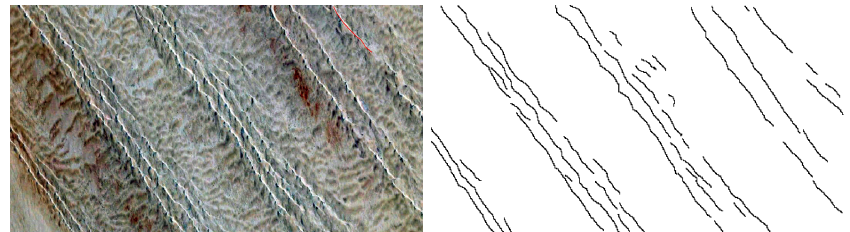
20 The first dataset is a small sample of a dozen satellite images from six separate desert regions on Earth (shown in Figure 1). Included are the Kalahari, Namib and Skeleton Coast sand sea regions in Namibia ([2]). Also represented in this dataset are the Simpson dune field in Australia, the Winnemucca Dune Complex in Nevada, and the White Sands National Monument. A wide range 25 of landform types are contained within each of these regions which provides a broad study for an automated crest-line detection method.

30 The Kalahari (fig. 1a)sands span from the southeastern region of Namibia to South Africa. The region is a 100-200 km wide and is composed of mostly fixed dunes [3]. Most of the area is comprised of simple linear form dunes, although some small areas contain some compound linear dunes as well. Unlike other desert regions, the Kalahari contains areas which are well vegetated. On average, the dunes range from 2m to 15m in height, with a 150m to 250m width, and spaced from 200m to 240m. These measurements may be useful for determining the reliability of our metric calculations.

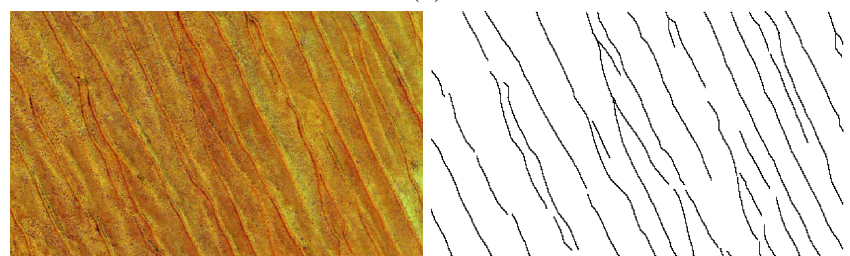
35 The Namib Sand Sea (fig. 1b) region spans approximately 34,000 km of the



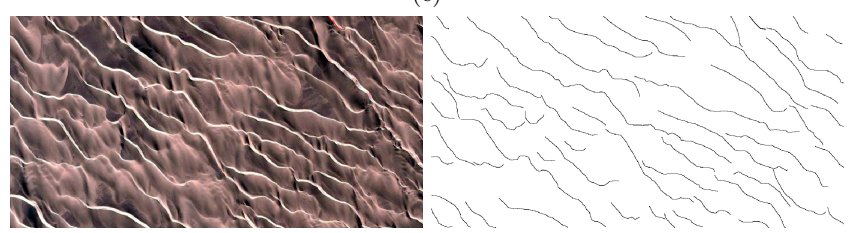
(a)



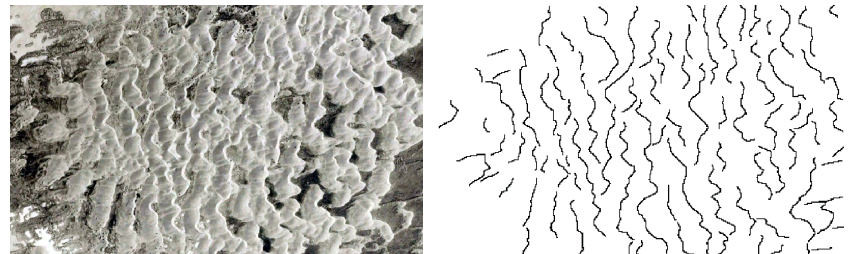
(b)



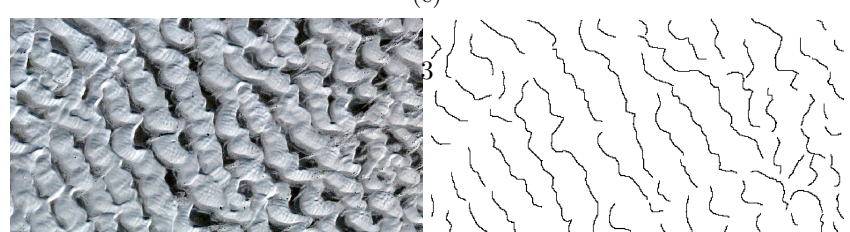
(c)



(d)



(e)



(f)

Altantic coast of Namibia, contains some of the largest and oldest sand dunes in the world according to [4]. High energy unimodal, bimodal and complex wind regimes create interesting dune field patterns in the Namib Sand Sea region of Namibia [5]. These wind patterns characterize the spatial variability of the 40 dune types, sizes, and other morphological properties of the region, making it an interesting case study for this research.

The Skeleton Coast (fig. 1d) dune field contains simple, locally compound, transverse and barchanoid dunes over its 2000 km² span according to [6]. The dunes pattern in this region are formed due to onshore winds and surface roughness changes between the dunes and coastal plains. The dune field is roughly aligned with the coast and is characterized with a large slip face in which dunes range from 20m to 80m in height. 45

Another region represented in the dataset is the Simpson (fig. 1c) dune field in Australia. Much like the Kalahari sands in southern Africa, the Simpson dune 50 fields contains many similar features. The areas are home to lush vegetation, and the dune field follow a mostly simple linear pattern where the dunes tend to be broad crested [7]. According to [8], some of the ridges continue unbroken for up to 200 km, where each crest measures 15m to 38m in height. The spacing between each crest varies depending on the height of the ridges. Areas with 55 larger ridges may have one or two dunes per kilometer, while smaller ridges may have five or six dunes per kilometer. These factor make this area an interesting addition to the dataset because the scale of the images is much larger.

Also present is the Winnemucca Dune Complex (WDC, fig. 1e) found in western United States, in Nevada. The WDC covers an area of roughly 900 60 km² north of Winnemucca, Nevada. The most common dune type present are stabilized parabolic dunes, but barchans and transverse ridges can also be found scattered throughout the area [9]. In fact, according to [10], the WDC is primarily covered by six crescentic complexes, a large sand sheet, and discontinuous sets of compound barchanbolic-parabolic dune fields. The WDC contains a 65 complex set of repetitive sequences of dunes which varying shapes and scales, which makes it an ideal candidate for this dataset.

Finally, the last area in the dataset is the White Sands National Monument (fig. 1f), located in the state of New Mexico, USA. This area boasts an interesting pattern of crescentic aeolian dunes which are formed in a systematically similar fashion to wind ripples and subaqueous dunes [11]. There are a wide range of features and properties in the White Sands dune field that merit study, such as described in [11]. These interactions include merging, lateral linking, defect repulsion, bedform repulsion, off-center collision, defect creation and dune splitting. The details of these interactions are outside the scope of this research but crest-line detection may be an essential preliminary step towards extracting those features. Measuring the number of dunes, crest lengths, defect density, dune spacing, and dune height are all done manually by experts in the field. A move towards an automated process would greatly improve research efforts, and would be a helpful tool for scientist in the field.

2.2. Mars Dataset

To verify the robustness of this approach, the method was also tested on another dataset which was used in [1]. The dataset provided is from the Ganges chasma on Mars, and includes satellite images, manually labeled crest-lines, and the results of the original author's method. The provided results lay a baseline benchmark for measuring quality and accuracy of crest-line detection algorithms. In order to more easily process the dataset, the Ganges region was split into sixteen areas of equal size, as shown in Figure 2. The ground truth included was not validated for correctness, the labeled data was used as-is, which may account for some errors (see Sections 4 and 5).

The dataset is essentially a CTX mosaic of the Ganges chasma, which spans an area of 500 km^2 , and includes a wide variety of dune types and morphologies. According to [12], many aeolian fatures can be found in the Ganges Chasma. Sand sheets, dune fields, unidirectional features such as barchan dunes were all identified within this region. overall structure of the Ganges dune field is a complex set of many diverging dunes, which makes it a challenging and appropriate area for testing this method.

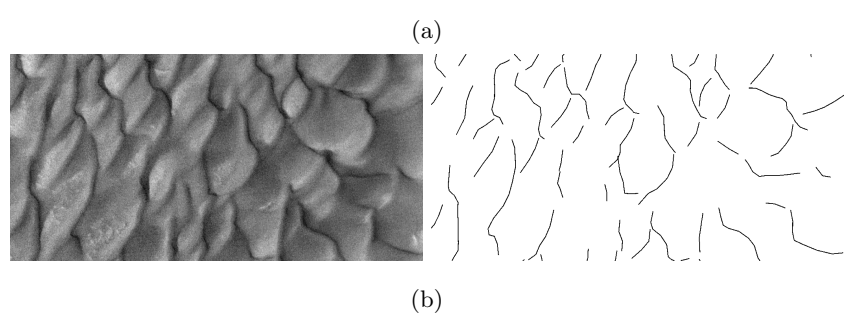
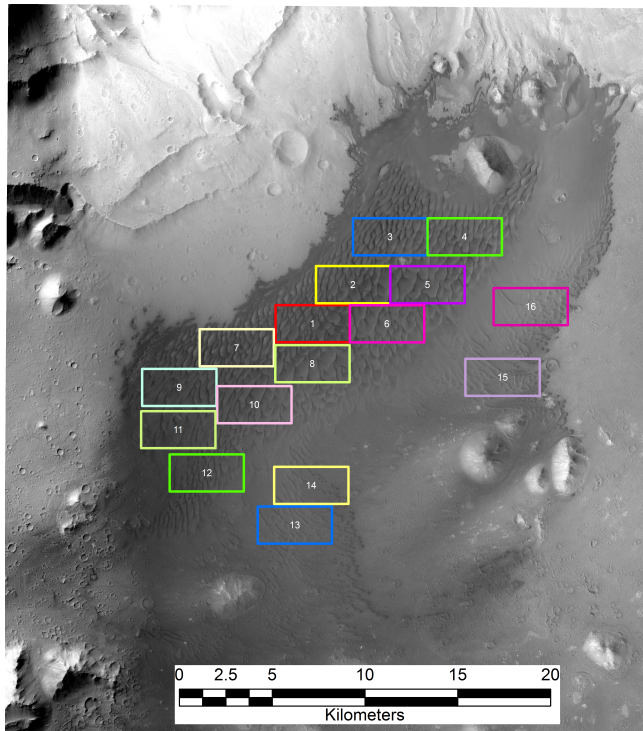


Figure 2: Ganges chasma Mars dataset from [1] which includes (2a) 16 regions extracted, (2b) sample image from region 1 with corresponding labeled ground truth

3. Methods

In this study, many different approaches were attempted and compared to extract meaningful features from the images and compute the appropriate morphological properties of the dune fields. The approach presented in this paper
100 can be summarized as a five stage process:

1. Image Preprocessing
2. Dominant Orientation Determination
3. Crest-line Candidate Detection
- 105 4. Validation
5. Metrics Calculations

3.1. Image Preprocessing

The pre-processing stage is an important step to normalize and de-noise the input data. Image processing is typically a low level process which attempts to
110 improve image quality, normalize illumination, or remove unnecessary information from the image. This type of processing will in turn improve higher level feature extraction.

The first step is to insure that the images have roughly the same scale. To enforce scale normalization, the datasets scales were manually selected for appropriate crest-line detection application, and the image resolutions were resized to roughly 1000 pixel in width. The appropriate resolution is chosen based on
115 a few factors:

- Source resolution: The selected resolution is limited by the original image's resolution. No extra information can be gained from increasing the source
120 image's resolution.
- Processing time: Higher resolution images require much more processing time overall which could be a limitation in a certain application.
- Scale selection: If the application's domain is found in a higher scale space, a higher resolution may not necessarily be required.

125 In this application, the goal is to detect the major crest-line, which is a higher scale domain, which means a higher resolution image is not a necessity. Note that some of the parameter selection in these processes are dependent on the resolution and scale of the images. In future work, dominant scale of the crest-lines could be determined automatically to improve the robustness of the 130 algorithms.

The next step in the process is to convert the images to gray scale. The images in the terrestrial, and Ganges datasets (described in section 2.1 and 2.2) are color images by default. Although color processing of these images has not extensively been tested as part of this study, it is arguable whether 135 using color information would improve the detection results. By converting the images to gray scale, an added benefit of normalizing the images across many region is implicitly enforced. Finally, the conversion process turns the three channel image into a single channel image which improves overall processing performance.

140 The final preprocessing step is to improve the image quality with low-pass filters. Many of the algorithms in this method rely on gradient information. Therefore, to extract the meaningful gradients, removing the highest frequencies (which in typically are responsible for noise), while preserving the lower scale or more desirable gradients. Two main popular filters are utilized. The 145 median filter, introduced in [13], is applied first to remove grain and salt and pepper noise while preserving important edges. In some cases, median filtering also helps remove some smaller scale objects such as bushes, trees, rocks, and other features which are indistinguishable from satellite images. Following is the standard Gaussian filter which removes the remaining high frequency noisy signals from the image. 150

An important aspect to note is the size of the filter masks, which is heavily dependent on the resolution of the input image. We found that in most cases, for images around 1000 pixels in width, a *sigma* value of approximately 1.5 and mask size of 7 by 7 was sufficient for this application. Once the image has 155 been preprocessed, the gradients can be computed and saved for future use.

Gradients can be computed by taking the first derivative of the image, using the popular Sobel operator.

An optional additional step is to apply histogram equalization to the image [14]. Poorly illuminated or low contrast images greatly benefit from histogram
160 equalization, because it stretches the contrast of the image in a consistent way. Using this process has shown to improve the overall results in many cases.

3.2. Dominant Orientation Determination

Computing the dominant orientation of the dune field is an important step in the process. The dominant orientation is the gradient direction of the crest-
165 lines to be detected. This process can help determine the average orientation of the dune field as well.

An important point to make is that this process could be optional if the dominant orientation is known a priori. Working with a dataset where the values are known improves the overall results of detection and enables skipping of this
170 step. In cases where this information is unknown, or unavailable, automated dominant orientation determination is a potential solution.

Typically, there exists a gradient peak at the crest-line peak of the dunes (although this may not always be the case for less pronounced dunes). The direction of the gradient should agree with the overall dominant orientation
175 of the dune field. Computing the dominant orientation of the field can be challenging in many cases because dunes typically have two major orientations, which are opposite directions. This phenomenon is clearly illustrated in Figure 3. The true crest-line peak, where the sunny side meets the shaded side is one gradient (fig. 3b). At the foot of the dune, where the shaded returns to light, a second gradient will be present, whom has an opposite direction (fig. 3a).

To remedy this issue, using histograms of gradient directions can be used to determine the true orientation. Histograms have been used for many processes and applications including [15, 16, 17]. Quantizing the space allows us to split edges according to their orientation, where each bin in the histogram represents
185 an edge orientation. Each bin then covers an angle of $\frac{2\pi}{N}$ radians, where N is

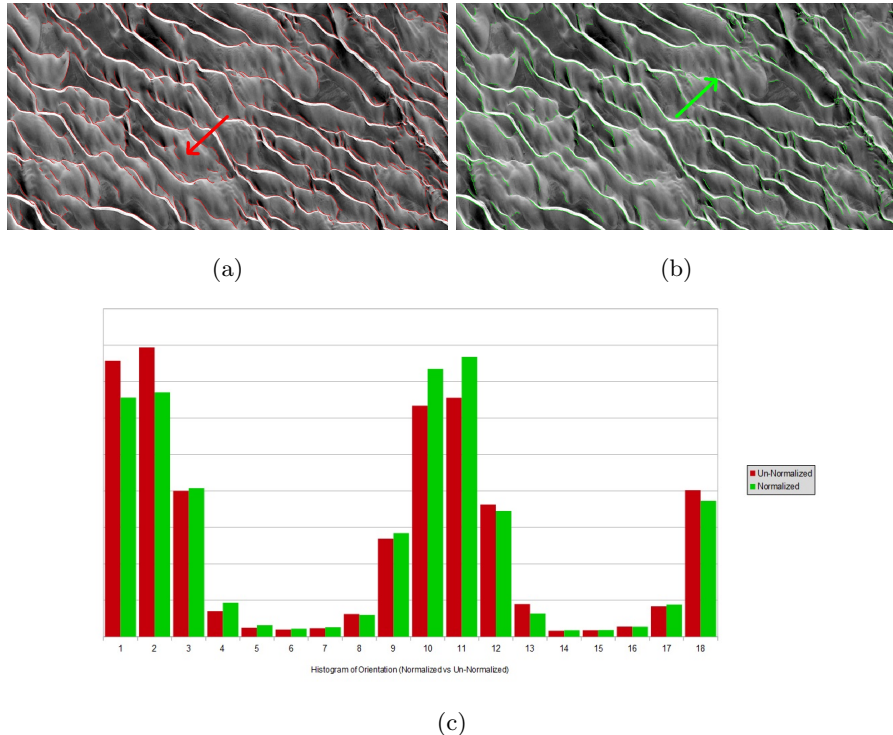


Figure 3: Results of unnormalized (red) and normalized (green) histograms of gradients ($N = 18$). The histogram contains two major peaks, but the crest-line is the weaker of the two peaks. (a) Edges which belong to the dominant orientation which are invalid crest-lines. (b) With normalization, the true crest-lines now have the higher overall magnitude. (c) The 18 bin histogram of gradients with and without normalization.

the number of bins. Each bin of the histogram is weighed by the magnitude of edges. Once the histogram is constructed, peaks in the magnitude will help determine the dominant orientation (ϕ) of the dune crest-lines. The approach poses two main problems:

- 190 1. Determining N : In practice, a larger value for N has shown to provide finer grain resolution which improves dominant orientation determination. In Figure 3 a value of $N = 18$ is used.
2. Multiple Peaks: Often, images may have multiple peaks in the histogram, but only one of the peaks should represent the true dominant orientation of crest-lines.
- 195 3. Global Solution: The computed dominant orientation is global to the image, which may not be optimal in cases of complex dune structures. A better solution would be to compute the dominant orientation in a local area of the image, to account for local shifts in orientation.

200 One assumption made is that the bin with the largest value represents the orientation of the crest-line edges. Although this assumption holds for many cases, it is not always the case. The Skeleton Coast test image provides a good example of this case in Figure 3. In this particular case, there are two major peaks in the histogram, where the stronger is not the part of the crest-line edge group, 205 and the weaker one is. Choosing the higher peak will cause invalid crest-lines to be chosen. In order to determine which peak best represents the crest-line edge group, some normalization can be applied. The normalization process begins by computing the mean vector of the gradients from the edge image as follows:

$$\hat{\mu} \langle \bar{x}, \bar{y} \rangle = \left\langle \frac{\sum_{i=0}^P \delta_{x_i}}{P}, \frac{\sum_{i=0}^P \delta_{y_i}}{P} \right\rangle$$

210 where P is the total number of detected edges from the Canny edge detector, δ_{x_i} and δ_{y_i} are the x and y gradient component of the i^{th} point. The mean orientation is computed from the mean vector as:

$$\theta_{\mu}^- = \arctan \left(\frac{\mu_{\bar{y}}}{\mu_{\bar{x}}} \right)$$

The gradients are then normalized by simply subtracting the mean vector from each gradient:

$$\dot{\delta}(x_i, y_i) = (\delta_{x_i} - \mu_{\bar{x}}, \delta_{y_i} - \mu_{\bar{y}})$$

The normalized orientation $\dot{\theta}_i$ can be computed:

$$\dot{\theta}_i = \arctan \left(\frac{\dot{\delta}_{y_i}}{\dot{\delta}_{x_i}} \right)$$

²¹⁵ To determine which bin the i^{th} edge point belongs to, we simply calculate $\left\lceil \frac{\dot{\theta}_{i,N}}{2\pi} - 0.5 \right\rceil$, and increment that bin by the magnitude of the normalized gradient by $\sqrt{\dot{\delta}_{x_i}^2 + \dot{\delta}_{y_i}^2}$. In essence, this normalization process removes the uneven skew of the gradients in the overall image. Removing this skew allows true crest-line edges to be fairly compared with other stronger edges. As shown in Figure ²²⁰ 3, the normalization process softens the stronger dominant edge and enhances the true crest-line edges. This process enables true crest-lines to be accurately determined in images where the valleys of dunes are sharp and contain strong edges.

²²⁵ Once the histogram is computed and normalized, the dominant orientation vector $\hat{\theta}_{dom}$ is determined by averaging the gradients belonging to the histogram bin with the highest value. With the dominant orientation knowledge acquired, candidate crest-line dunes can be detected.

3.3. Crest-line Candidate Detection

²³⁰ The goal of the initial candidate detection step is to find as many of the true crest-lines as possible. For optimal results, candidate detections should span as much of the crest-line as possible and ideally be a single contiguous segment. These constraints help improve the overall accuracy and compute the geomorphological properties of the dune fields.

The candidate detection process can be summarized in four steps:

- ²³⁵ 1. Compute the gradient orientation image relative to the dominant orientation.

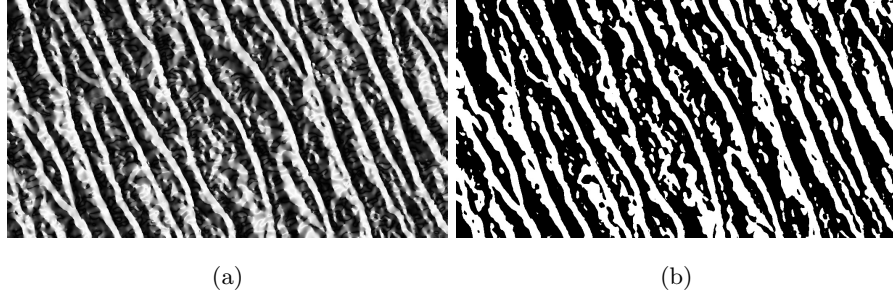


Figure 4

2. Threshold the gradient orientation image to preserve all pixels which agree with the dominant orientation.
3. Find the contours of the thresholded regions of the gradient orientation image.
- 240 4. Shift the contours to the nearest gradient magnitude peak.

The relative gradient orientation image maps the gradient directions relative to the computed dominant orientation. This can be achieved by taking the dot product of the normalized gradient vectors, with the normalized dominant orientation vector at each pixel location on the image, as shown below.

$$R_{\theta_{ij}} = \hat{\delta}_{ij} \cdot \hat{\theta}_{dom}$$

In essence, the resulting image R_θ displays maps the gradient direction vectors to a single value with a range of values from -1 to $+1$. A brighter pixel then *agrees* with the dominant orientation while dark pixels *disagrees* with it.

- 245 5. The resulting transformation is shown in Figure 4.

The benefit of this transformation is that due to the nature of the domain problem, this produces bright regions around dune crest-lines. Another benefit is that it much less sensitive to weaker

4. Results

- 250 6. There are various bibliography styles available. You can select the style of your choice in the preamble of this document. These styles are Elsevier styles

based on standard styles like Harvard and Vancouver. Please use BibTeX to generate your bibliography and include DOIs whenever available.

5. Discussion

²⁵⁵ 6. Conclusions

References

- [1] M. B. L. F. T. M. David Vaz, Pedro Sarmento, Object-based dune analysis: Automated dune mapping and pattern characterization for ganges chasma and gale crater, mars, Geomorphology (250) (2015) 128–139.
- ²⁶⁰ [2] A. S. Goudie, Desert landforms in namibia - a landsat interpretation.
- [3] N. Lancaster, Development of linear dunes in the southwestern kalahari southern africa, Journal of Arid Environments (1987) 233–244.
- [4] A. S. Goudie, Namib sand sea: Large dunes in an ancient desert.
- ²⁶⁵ [5] N. Lancaster, Winds and sand movements in the namib sand sea, Earth Surface Processes and Landforms 10 (1985) 607–619.
- [6] N. Lancaster, Dunes on the skeleton coast, namibia (south west africa): Geomorphology and grain size relationships, Earth Surface Processes and Landforms 7 (1982) 575–587.
- ²⁷⁰ [7] P. P. Hesse, The australian desert dunefields: formation and evolution in an old, flat, dry continent.
- [8] C. R. Twidale, The simpson desert, central australia, South African Geographic Journal 65 (1980) 3–17.
- [9] S. H. W. James R. Zimbelman, Eolian dunes and deposits in the western united states as analogs to wind-related features on mars.

- 275 [10] N. Pepe, The geomorphology, eolian activity, and petrology of the win-
nemucca dune complex, humboldt county, nevada, usa, Ph.D. thesis, Uni-
versity of Nevada, Reno.
- 280 [11] G. A. K. Ryan C. Ewing, Aeolian dune interactions and dune-field pattern
formation: White sands dune field, new mexico, *Sedimentology* 57 (2010)
1199–1219.
- [12] R. A. B. L. K. Fenton, T. I. Michaels, Aeolian sediment sources and trans-
port in ganges chasma, mars: Morphology and atmospheric modeling, 2012.
- [13] A fast two-dimensional median filtering algorithm, *IEEE Transactions on
Acoustics, Speech, Signal Processing* 27 (1) (1979) 13–18.
- 285 [14] R. E. W. R. C. Gonzalez, *Digital Image Processing*, 2008.
- [15] D. G. Lowe, Distinctive image features from scale-invariant keypoints, *International Journal of Computer Vision*.
- [16] B. T. N. Dalal, Histograms of oriented gradients for human detection,
CVPR (2005) 886–893.
- 290 [17] J. C. Rui Hu, Mark Barnard, Gradient field descriptor for sketch based
retrieval and localization, *2010 IEEE International Conference on Image
Processing* (2010) 1025–1028.